



Hydrazine hydrate and tartaric acid corrosion inhibitor as a high efficiency corrosion inhibitor for marine engineering and mechanism study

Tiantian Shu^a, Xuefan Gu^b, Xuewen Cao^c, Yefei Wang^c, Ying Tang^b, Zhongying Xu^{a,c,*}

^aState Key Laboratory of Petroleum Pollution Control, Xi'an Shiyou University, Xi'an 710065, China, emails: b22060008@s.upc.edu.cn (Z. Xu), 1289816716@qq.com (T. Shu)

^bState Key Laboratory of Petroleum Pollution Control, Shaanxi Province Key Laboratory of Environmental Pollution Control and Reservoir Protection Technology of Oilfields, Xi'an Shiyou University, Xi'an 710065, China, emails: xuefangu@xsyu.edu.cn (X. Gu), tangying78@xsyu.dedu.cn (Y. Tang)

^cChina University of Petroleum (Huadong), Qingdao 266580, China, emails: caoxw@s.upc.edu.cn (X. Cao), wangyf@upc.edu.cn (Y. Wang)

Received 2 March 2023; Accepted 23 August 2023

ABSTRACT

Rapid corrosion of steel bars in marine and complex saline environments has become a serious concern, and corrosion inhibitor for steel bar has proved to be one of the main protective measures to prevent the corrosion. In this paper, a new organic composite anti-corrosion agent (HTCI) was synthesised by hydrazine hydrate and tartaric acid for the preventing reinforced concrete from corrosion in marine engineering. The inhibition behaviors of HTCI for Q235 steel in saturated Ca(OH)₂ solution with 3.0 wt.% NaCl were studied by weight loss, electrochemical measurement and surface analysis. All these techniques revealed that inhibition efficiency increased with increasing HTCI concentration and the inhibitor showed 84.37% inhibition efficiency at a concentration of 500 mg·L⁻¹. Potentiodynamic polarization studies indicated the HTCI with mixed-type inhibitor properties. Scan analysis demonstrated that the depth of the pitting crater decreased with increasing HTCI concentration. Kinetically and thermodynamically simulated that the adsorption of HTCI on mild steel obeys Langmuir adsorption isotherm, and the mechanisms of this corrosion inhibitor were based on physical and chemical adsorption.

Keywords: Corrosion inhibitor; Weight loss; Langmuir adsorption isotherm; Electrochemical techniques; Surface studies

1. Introduction

With the development of marine economy and marine high-tech, more and more reinforced concrete composite materials are applied to marine engineering construction. The factors on the service life of reinforced concrete structures include corrosion of coarse reinforcement, carbonization of concrete structures, freeze-thaw damage, alkali-aggregate reaction and chemical erosion among them [1,2], and corrosion of reinforcement is the primary factor that accelerates the destruction of concrete structures [3]. At present, the corrosion and protection of reinforced concrete

structures have become a widespread concern and research problem in the world. The corrosion of reinforcing steel in concrete structures is mainly caused by damage to the passivation film on the surface of the reinforcing steel, especially the carbonation of the concrete and the invasion of chloride ions. Fundamentally, the primary problem to be solved in the protection of reinforced concrete structures is the corrosion and corrosion technology of the reinforcement, which should significantly improve the corrosion resistance of the concrete itself against the reinforcement. Corrosion inhibitor is mixed into cement or mortar in small quantities and can effectively inhibit or delay the occurrence of corrosion and at the same time reduce the

* Corresponding author.

corrosion rate of reinforcing steel. The addition of corrosion inhibitors to reinforcing steel has become a major protective measure against the corrosion of reinforcing steel. As an effective measure to prevent long-term corrosion of reinforcing steel, it is inexpensive and simple to operate for engineering construction and increasingly widely used [4].

Although many anti-corrosion interventions have been developed and used, there are still some shortcomings [5]. (1) Most corrosion protection processes at this stage are measured to focus on the protection of the surface, and for complex structures or exposure to harsh environmental conditions, these measures are often ineffective, as surface breakage or sealing defects may still lead to corrosion. (2) Lack of long-term performance, certain anti-corrosion interventions show good anti-corrosion performance at the beginning, but over time, their effectiveness will gradually weaken. (3) High treatment costs, some efficient anti-corrosion interventions require complex treatment steps, specialized equipment and high-cost materials. This makes it difficult to spread in some large-scale applications. (4) Limited by material selection, current anti-corrosion interventions are often limited to specific materials or applications under specific environmental conditions. However, actual projects often use multiple materials and suffer from multiple environmental influences, such as water, chloride ions, acidic or alkaline conditions, etc. (5) Environmental friendliness, some traditional anti-corrosion interventions may use chemicals that are harmful to the environment, such as heavy metals or organic solvents. For projects pursuing sustainable development and environmental friendliness [6].

In recent years, countries have been working on the development of new and efficient corrosion inhibitors [7]. Corrosion inhibitors in this paper were classified into anodic corrosion inhibitors, cathodic corrosion inhibitors and composite corrosion inhibitors according to their different working mechanisms [8]. Composite corrosion inhibitors inhibit both anodic and cathodic reactions and form a thin protective hydrophobic film over the entire surface of the metal through an adsorption mechanism, thus reducing the corrosion rate. The main application methods for composite corrosion inhibitors are as admixtures added to fresh concrete, applied to hardened concrete and damaged structures, added to repair mortars and used for surface treatment of reinforcement before concrete placement [9]. Migration corrosion inhibitor (MCI) is a complex corrosion inhibitor that diffuses through the gas and liquid phases of the concrete pores to form a protective film on the surface of the reinforcement and acts as a corrosion inhibitor. Malik et al. [10] reported a type of MCI, a mixture of surfactant and amine salts in water, which can be used both on concrete surfaces and as a corrosion inhibitor for reinforcement. Saxena et al. [11] showed that MCI based on amino carboxylate chemistry is the most effective in terms of simultaneous anodic and cathodic interactions. Raja et al. [12] review the types of corrosion inhibitors that may work in concrete and the mechanism of Cl^- attack on concrete, including that amines, alkylamines, amino acids, monocarboxylates, polycarboxylates, amino alcohols, organic heterocyclic compounds and green products can be successful [13].

Future research and technological development should focus on addressing these issues to improve the effectiveness,

durability, economy and environmental friendliness of corrosion protection measures to better protect engineering structures from corrosion. The inhibitors available on the market cannot simultaneously meet the requirements of corrosion resistance and early strength of reinforced concrete under seawater conditions. Therefore, it is important to study the law and mechanism of corrosion of reinforcing steel in concrete under complex marine environment, to prepare environmentally friendly, low cost and effective corrosion inhibitors for reinforcing steel, to study the evolution of concrete deterioration and to improve the durability of concrete.

In this study, a new composite corrosion inhibitor (HTCI) was synthesized from hydrazine hydrate and tartaric acid. The influence of HTCI on the corrosion behavior of Q235 steel in saturated $\text{Ca}(\text{OH})_2$ containing 3.0 wt.% NaCl was studied by weight loss method, electrochemical experiment, surface morphology analysis, thermodynamic and kinetic analysis, etc. The results proved that the composite corrosion inhibitor with salt resistance, high-temperature resistance, low cost and environmental protection in the marine environment. It has good adsorption on the surface of reinforcement, and has weak adsorption of inhibitor molecules on the surface of cement particles.

2. Experimental set-up

2.1. Materials

All the chemicals and solvents used were of analytical grade and utilized without further purification. NaOH and CaO were purchased from Tianjin Damao Chemical Reagent Factory, Tianjin, China; anhydrous ethanol and hydrazine hydrate were supplied from Tianjin Fuyu Fine Chemical Co., Ltd., Tianjin, China; tartaric acid used are from Tianjin Comio Chemical Reagent Factory, Tianjin, China; Q235 steel sheet purchased from Shanghai Lok Song Mechahhta al & Electrical Equipment Co., Ltd., Shanghai, China; The model HH-2 electric thermostatic water bath was purchased from Beijing Kewei Yongxing Instruments Co., Ltd., Beijing, China; the model DZF-18 electric blast dryer was provided by Shanghai Keheng Industrial Development Co., Ltd., Shanghai, China; the electrochemical workstation Model CS350 was from Wuhan Coster Instruments Co., Ltd., Wuhan, China; the model DSX500 automatic 3D imaging microscope used was purchased from Olympus Corporation, Beijing, China.

2.2. Weight loss studies

Q235 mild steel was purchased from Shanghai Mechanical & Electrical Equipment Co., and the coupons, content and properties of Q235 used in this experiment are shown in Tables 1 and 2. The dimensions of Q235 specimen used for weight analysis were $40 \text{ mm}^3 \times 2 \text{ mm}^3 \times 13 \text{ mm}^3$. To obtain reliable and accurate research results, all Q235 mild steel specimens were subjected to a pretreatment, it was necessary to use different grades (280–360–600–1,000) of sandpaper to remove corrosion particles. After that, mild steel was degreased with acetone and then wiped with anhydrous ethanol and blown dry in cold air.

The weight loss study was carried out at room temperature for 7 d in saturated $\text{Ca}(\text{OH})_2$ solution with 3.0 wt.% NaCl.

The uniform corrosion rates (V) is shown by Eq. (1) and the inhibition efficiency (η) [14] is determined in Eq. (2) [15]:

$$V = \frac{8.76 \times 10^4 \times W}{S \times t \times \rho} \quad (1)$$

where W is the weight loss value, S is corrosion area of steel sheet, t is corrosion time and ρ is density of steel sheet about $7.85 \text{ g}\cdot\text{cm}^{-3}$.

$$\eta = \frac{M_0 - M}{M_0} \times 100\% \quad (2)$$

where M_0 and M are the weight loss values of mild steel without and with the inhibitor, respectively.

2.3. Synthesis of HTCI and corrosive medium

Hydrazine hydrate and tartaric acid corrosion inhibitors (HTCI) are based on the reducing properties of hydrazine hydrate and the coordination effect of tartaric acid. The basic theory is to inhibit metal corrosion reactions by generating protective films and forming physical barriers. This system is widely used in the field of metal corrosion control and protection in practical applications.

The inhibitor of HTCI was made by 1:1 tartaric acid:hydrazine hydrate, the temperature is 25°C , the speed is 2,000 rpm in the beaker continuous reaction and stirring

Table 1
Q235 mild steel sheet composition content

| Coupons | Content (%) |
|---------|--------------|
| C | 0.16 |
| Si | 0.26 |
| Mn | 0.15 |
| P | ≤ 0.015 |
| S | ≤ 0.09 |
| Al | — |
| Cr | 0.02 |
| Ni | 0.025 |
| Cu | 0.024 |

Table 2
Q235 mild steel sheet tensile and process properties

| | |
|------------------------------------|------|
| Tensile strength (b/Mpa) | 425 |
| Yield strength (0.2/Mpa) | 310 |
| Elongation (5%) | 35 |
| Density (g/cm^3) | 7.85 |

for 1 h. The reaction equations involved in the synthesis process are as shown in Fig. 1.

Simulated concrete pore solution with chloride environmental processes: First dissolve about 1 g of CaO in 1,000 mL of tap water, when a precipitate appears at the bottom of the beaker, that is, the solution in the beaker is saturated $\text{Ca}(\text{OH})_2$ solution. The saturated $\text{Ca}(\text{OH})_2$ solution is filtered using a circulating vacuum pump to remove the sediment. Then, 30 g of NaCl was added to the filtered solution, stirred and dissolved in a 1,000 mL volumetric flask, and the saturated $\text{Ca}(\text{OH})_2$ simulated concrete pore solution with chloride containing 3.0 wt.% NaCl needed to be ready to use. Additionally, the concentration of the inhibitor (HTCI) used ranged from 100 to 1,000 $\text{mg}\cdot\text{L}^{-1}$.

2.4. Electrochemical studies

Electrochemical workstation (CS350, Wuhan Coster Instruments Co., Ltd.) was used for electrochemical testing. Using the CorrTest electrochemical test system for corrosion monitoring by linear polarization and weak polarization, which can continuously measure the instantaneous corrosion rate of materials. A three-electrode test system was used. The reference electrode, the auxiliary electrode and the working electrode were saturated calomel electrode, the platinum electrode and the self-made Q235 steel, respectively. The relevant electrochemical parameters were determined by potentiodynamic polarization experiments and impedance spectroscopy tests, and the electrochemical parameters were analyzed using Z-view software [16].

Firstly, steady-state polarization was selected in the test method, and open-circuit monitoring was performed for 8 h. As shown in Fig. 2, the open-circuit potential varied within ± 5 –10 mV within 1 h and was considered stable [17].

Potentiodynamic polarization measurements [18] were performed at a scan rate of $0.5 \text{ mV}\cdot\text{S}^{-1}$. The mild steel surface was exposed to various concentrations of inhibitors in 250 mL of $\text{Ca}(\text{OH})_2$ solution with 3.0 wt.% NaCl at room temperature. The inhibition efficiency (IE %) was calculated using Eq. (3):

$$\text{IE}(\%) = \frac{i_{\text{corr}}^0 - i_{\text{corr}}}{i_{\text{corr}}^0} \times 100 \quad (3)$$

where i_{corr}^0 and i_{corr} are the corrosion current density without and with the inhibitor, respectively.

Impedance measurements were carried out in the frequency range from 0.01 to 100 kHz, Excitation sine wave signal amplitude is 10 mV with an AC signal at the open-circuit potential. The Nyquist and Bode plots [19] are generally used to represent the impedance spectrum form. The percentage inhibition efficiency was calculated from Eq. (4):

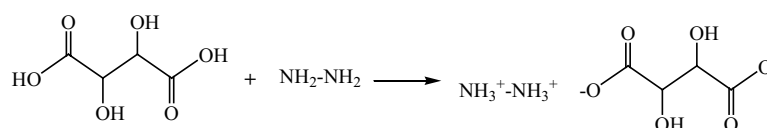


Fig. 1. General procedure for the synthesis of HTCI.

$$E_{R_p} = \frac{R_p - R_p^0}{R_p} \times 100\% \quad (4)$$

where R_p and R_p^0 are the charge transfer resistance of mild steel with and without inhibitor, respectively.

2.5. Surface studies

In the present study, DSX-500 (Olympus, Tokyo, Japan) fully automatic 3D imaging microscope was used to scan the steel surface before and after corrosion in bright field (BF) mode, 2D, height and 3D images were acquired simultaneously to analyze the association between image data information and corrosion morphology features. The scanning areas of steel coupons were $5 \mu\text{m} \times 5 \mu\text{m}$.

3. Results and discussion

3.1. Weight loss measurements

The effects of different concentrations of corrosion inhibitors on the corrosion inhibition of Q235 mild steel in

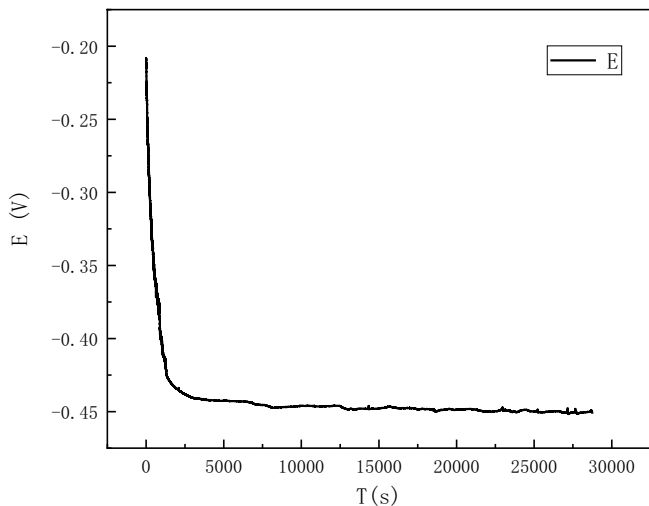


Fig. 2. Open circuit potential vs. time for 8 h monitoring.

saturated $\text{Ca}(\text{OH})_2$ solution with 3.0 wt.% NaCl at 303 K were investigated via the weight loss methods for 3 and 7 d. The corrosion rates and inhibition efficiency are shown in Fig. 3. It shows that at 3 d the inhibition efficiency increased with increasing HTCI concentration at 100–400 $\text{mg}\cdot\text{L}^{-1}$. However, when the concentration exceeds 400 $\text{mg}\cdot\text{L}^{-1}$ the inhibition efficiency starts to decrease and the inhibition rate starts to increase. It shows that at 7 d inhibition efficiency rose up with the increase in the HTCI concentration and the maximum inhibition efficiency of HTCI was 84.37%. On the contrary, the inhibition rate decreased with the increase in inhibition concentration, the minimum inhibition rate was $0.00524 \text{ mm}\cdot\text{a}^{-1}$ at 500 $\text{mg}\cdot\text{L}^{-1}$ [20].

3.2. Effect of temperature

Fig. 4 shows effect of HTCI on corrosion rate of Q235 carbon steel at different temperatures for 7 d. The reason for the gradual decrease of the corrosion rates may be the observed balance of absorption and desorption of HTCI molecules on the surface of Q235 carbon steel with the increase of temperature.

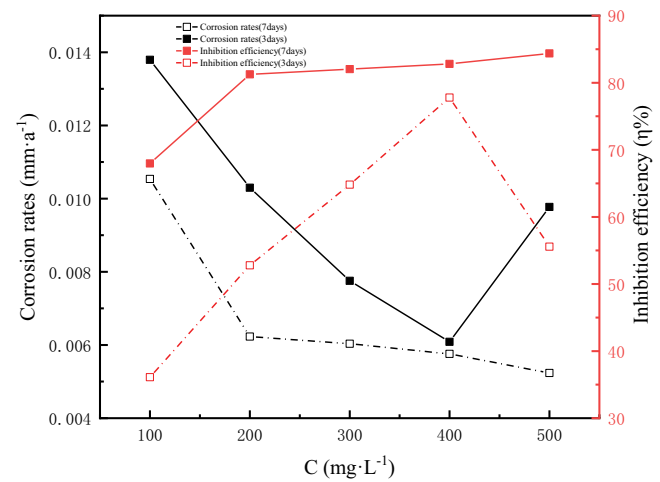


Fig. 3. Experimental results of HTCI weight loss method at 303 K for 3 and 7 d.

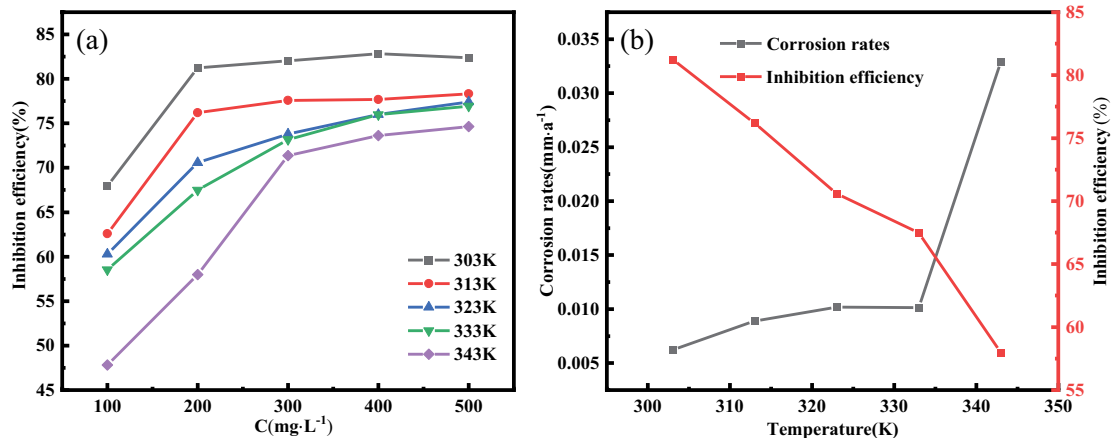


Fig. 4. Effect of temperature on corrosion inhibition performance of HTCI for 7 d.

Fig. 4a visually represents the corrosion rates of different concentrations of HTCI in saturated $\text{Ca}(\text{OH})_2$ solution with 3.0 wt.% NaCl at different temperatures. The corrosion rate decreased with an increase at different temperatures. Fig. 4b is a comparison of the corrosion rate of HTCI at $500 \text{ mg}\cdot\text{L}^{-1}$ at different temperatures. The results showed that the corrosion rates of Q235 carbon steel gradually decreased with the increase in temperature. The corrosion rate was $0.01015 \text{ mm}\cdot\text{a}^{-1}$ at the temperature of 333 K, and $0.03294 \text{ mm}\cdot\text{a}^{-1}$ at the temperature of 343 K, which was probably because the passivation film generated by HTCI on the metal surface was destroyed due to the high temperature and the corrosion rates increase. The surface of Q235 changes complexly under the influence of temperature, and the mechanism of corrosion inhibitor action can be inferred by further calculation of thermodynamic parameters.

3.3. Effect of time

The inhibition efficiency of Q235 steel in saturated $\text{Ca}(\text{OH})_2$ solution with 3.0 wt.% NaCl with time at 303 K is shown in Fig. 5. The maximum inhibition efficiency of 82.92% for 7 d and the minimum corrosion rate of $0.00524 \text{ mm}\cdot\text{a}^{-1}$. The corrosion rate decreases evidently with an increase in inhibitor time. The hydroxyl group ($-\text{OH}$), the carboxylic acid ($-\text{COO}^-$) and the amino group ($-\text{NH}_2$) in hydrazine hydrate were adsorbed on the metal surface by coordination. Polar terminus of these group were close to the metal, while the outward water-repellent terminus slow down the corrosion. Therefore, the maximum corrosion rate was 83.47% and 85.41% for 14 and 30 d, respectively, and the minimum corrosion rate was 0.0069 and $0.00637 \text{ mm}\cdot\text{a}^{-1}$, respectively.

3.4. Potentiodynamic polarization studies

The potentiodynamic polarization curves for mild steel in saturated $\text{Ca}(\text{OH})_2$ solution with 3.0 wt.% NaCl containing different concentrations of the investigated HTCI are shown in Fig. 6. Table 3 shows that the values of anodic Tafel slope (β_a), cathodic Tafel slope (β_c), corrosion current

densities (i_{corr}), corrosion potential (E_{corr}) and inhibition efficiency (IE %) calculated at different concentrations using potentiodynamic polarization. Fig. 6 shows that the Tafel slope of both cathodic and anodic changed with increasing

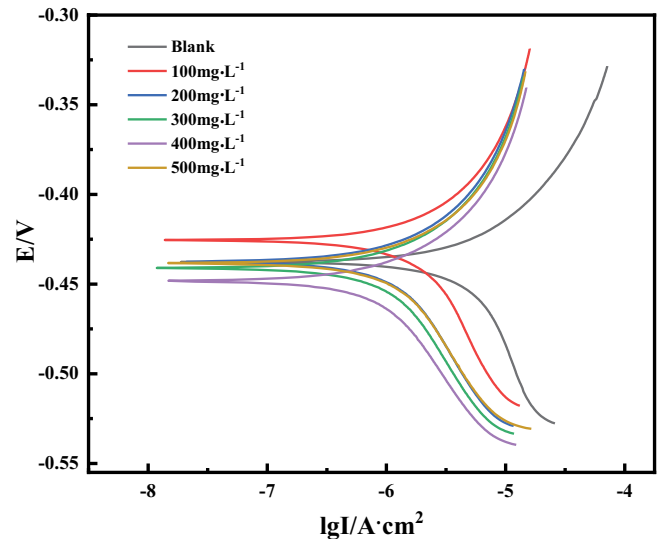


Fig. 6. Tafel polarization curves of HTCI at different concentrations.

Table 3

Fitting results of polarization curve parameters at different concentrations

| $c \text{ (mg}\cdot\text{L}^{-1})$ | $\beta_a \text{ (mV)}$ | $\beta_c \text{ (mV)}$ | $i_{\text{corr}} \text{ (}\mu\text{A}\cdot\text{cm}^{-2})$ | $E_{\text{corr}} \text{ (V)}$ | IE (%) |
|------------------------------------|------------------------|------------------------|--|-------------------------------|--------|
| 0 | 248.03 | 689.45 | 13.46 | -0.5537 | – |
| 100 | 293.82 | 1,380.14 | 9.78 | -0.4255 | 27.37 |
| 200 | 192.72 | 629.54 | 5.99 | -0.4376 | 55.49 |
| 300 | 166.28 | 544.49 | 4.71 | -0.4409 | 65.01 |
| 400 | 141.52 | 412.03 | 3.61 | -0.4483 | 73.18 |
| 500 | 184.54 | 560.20 | 5.82 | -0.4384 | 56.76 |

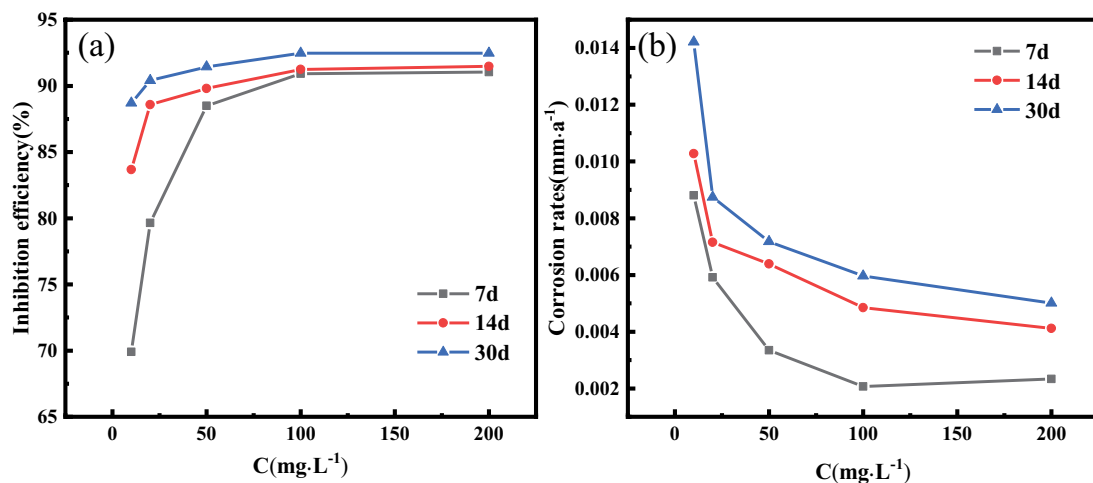


Fig. 5. Effect of time on corrosion inhibition performance of HTCI at 303 K.

HTCI concentration, which indicates that HTCI inhibitor prevents carbon steel from being corroded by inhibiting the anode at lower concentrations, and prevents corrosion mainly by inhibiting the cathode between 200–500 mg·L⁻¹ concentrations. This indicated that the HTCI inhibitor had comprehensive effects and it controls both cathodic and anodic parts.

The data in Table 3 reveal that the anodic Tafel slope (β_a) gradually decreased with increasing concentration. At first, the cathodic Tafel slope (β_c) increased in an inhibitor HTCI concentration of 100 mg·L⁻¹ and then began to decrease. The corrosion current densities (i_{corr}) decreased from 13.46 to 5.82 $\mu\text{A}\cdot\text{cm}^{-2}$. The inhibition efficiency (IE %) vs. the inhibitor concentration of HTCI is also presented in Table 3 and decreased most obviously when the concentration of HTCI was 500 mg·L⁻¹. Combined with the results of a weight loss experiment with a reaction time of 3 d, this decreased corrosion rates was caused by the diminished synergistic effect of hydrazine hydrate and tartaric acid. The increase in tartaric acid and hydrazine hydrate molecule made shifted the estimated E_{corr} value towards the negative value, so the HTCI had the corrosion inhibition effect on mild steel at 303 K.

3.5. Electrochemical impedance spectroscopy

The Nyquist representations of impedance behavior of mild steel in saturated Ca(OH)₂ solution with 3.0 wt.% NaCl with and without addition of different concentrations of inhibitor are shown in Fig. 7. It can be seen that the scanning result of HTCI inhibitor is a single capacitive loop via scanning the electrochemical impedance spectrum. The larger radius of the capacitive loop indicated more prominent corrosion resistance during the electrochemical reaction process. The radius of the capacitive loop decreased at a concentration of 500 mg·L⁻¹, the result was in acceptable agreement with those obtained from weight loss study and shown the same trend [21].

Furthermore, the measured impedance data were analyzed by fitting based on the equivalent circuit given in Fig. 8 [22]. A standard Randall circuit was used to analyze

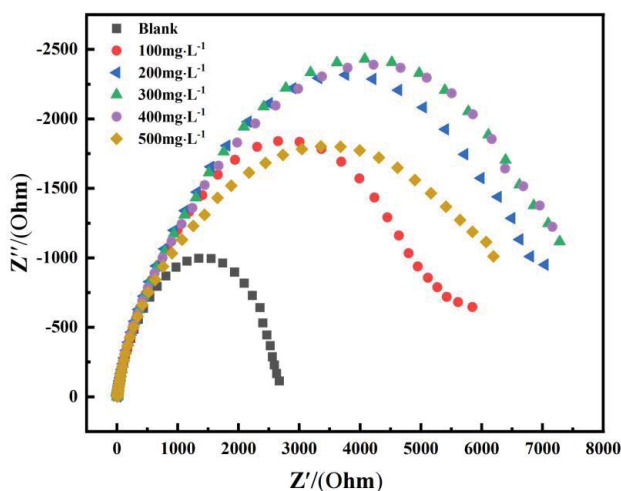


Fig. 7. Nyquist impedance spectra of HTCI different concentrations.

the impedance spectrum containing a single capacitive semicircle, where the circuit consists of a solution resistance component (R_s), a charge transfer resistance (R_p) and a capacitance component (CPE). CPE is a long phase angle equivalent element that is used to describe the bilayer deviation from the pure capacitance C. CPE-T and CPE-P are the 2 parameters expressed, where CPE-T represents the bilayer capacity and CPE-P represents the dispersion effect index, it is equivalent to the dispersion factor.

The values of R_p in Table 4 indicated that CPE-P had a brought downtrend when concentrations of the compound increased in the solution. With the value of CPE-P decreasing, the double electric layer thickness increased and the dispersion index reduced. Moreover, the corrosion inhibition effect of HTCI gradually increased with the increase in concentration. The corrosion rate, reaching its maximum value, of 70.25% at 400 mg·L⁻¹ of HTCI was consistent with the results obtained by electrolysis and a short time (3 d) weightlessness experiment.

3.6. Adsorption isotherm and kinetic parameters

The interaction of inhibitor molecules with the surface of carbon steel was studied by the adsorption isotherms and thermodynamic calculations [23]. Adsorption involved two phases and this separation process with certain components can be described by physical adsorption or chemical adsorption [24–27]. The adsorption characteristics of the corrosion inhibitors on the surface of carbon steel can be provided by various adsorption isotherm, including those of Langmuir, Temkin and Frumkin. The expressions of the three adsorption theories [28,29].

The Langmuir adsorption isotherm can be calculated as Eq. (5) [30]:

$$\frac{c}{\theta} = \frac{1}{K} + C \tag{5}$$

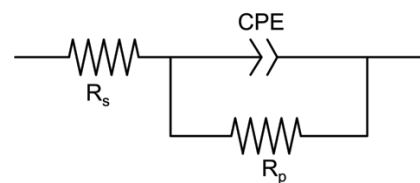


Fig. 8. Equivalent circuit for impedance measurements.

Table 4 Fitting results of polarization curve parameters at different concentrations

| c (mg·L ⁻¹) | R _s (Ω·cm ⁻²) | CPE-T (μF·cm ⁻²) | CPE-P (μF·cm ⁻²) | R _p (Ω·cm ⁻²) | E _{RP} (%) |
|-------------------------|--------------------------------------|------------------------------|------------------------------|--------------------------------------|---------------------|
| 0 | 7.494 | 1.0472 × 10 ⁻⁴ | 0.8338 | 2,610 | – |
| 100 | 8.089 | 1.1748 × 10 ⁻⁴ | 0.7857 | 5,366 | 51.36 |
| 200 | 6.660 | 1.2885 × 10 ⁻⁴ | 0.7783 | 6,734 | 61.24 |
| 300 | 5.778 | 1.3185 × 10 ⁻⁴ | 0.7787 | 7,960 | 67.21 |
| 400 | 5.442 | 1.3953 × 10 ⁻⁴ | 0.7808 | 8,773 | 70.25 |
| 500 | 5.524 | 1.1882 × 10 ⁻⁴ | 0.7811 | 5,559 | 53.05 |

The Temkin adsorption isotherm was determined by Eq. (6):

$$\exp(-2a\theta) = Kc \quad (6)$$

The Frumkin adsorption isotherm was calculated using Eq. (7) [31]:

$$\frac{\theta}{1-\theta} \exp(-2a\theta) = Kc \quad (7)$$

where c denotes the concentration of corrosion inhibitor, θ is the surface coverage, which is considered here as the corrosion inhibition rate like η , K denotes the equilibrium constant of the adsorption process, and is the mutual attraction between adsorbed particles.

The adsorption performance of HTCI was investigated using three different adsorption isothermal models (Langmuir, Temkin and Frumkin) as shown in Fig. 9. The linear regression coefficient (R^2) of Langmuir adsorption isotherm (Fig. 9a), Temkin type (Fig. 9b) and Frumkin type (Fig. 9c) were 0.998, 0.9158, and 0.8591, respectively. Among the three isothermal models, the HTCI inhibitor most obeyed the Langmuir adsorption isotherm. The ammonium ions ($-\text{NH}_4$) and hydroxyl group ($-\text{OH}$) in HTCI were adsorbed on the metal surface, forming a uniform adsorption film

on the carbon steel surface to isolate the corrosion medium from the metal surface and restrain the corrosion. At the same time, to fit the degree of surface coverage (θ , shown in Fig. 9d) at different temperatures. The HTCI at different temperatures all obeyed the Langmuir adsorption isotherm, and the strong correlation ($R^2 \geq 0.99$) at different temperatures confirms the effectiveness of the model.

The Langmuir adsorption isotherm model was used to further determine the adsorption equilibrium constant (K). The K value is related to the standard free energy of adsorption (ΔG_{ads}). ΔG_{ads} value is calculated using Eq. (8), where R is the universal gas constant, $R = 8.314 \text{ J}\cdot\text{K}^{-1}\cdot\text{mol}^{-1}$. T is the temperature, 55.5 is the concentration of water in solution, $\text{mol}\cdot\text{L}^{-1}$ [32]. The thermodynamic parameters of theoretical adsorption are given in Table 6. Table 5 shows that the negative value of ΔG_{ads} indicated that adsorption of HTCI on the surface of the Q235 steel sheet was a spontaneous process. The absolute value of ΔG_{ads} was related to the type of adsorption. When the value of ΔG_{ads} is less than or equal to $20 \text{ kJ}\cdot\text{mol}^{-1}$, physical adsorption associated with an electrostatic attraction between the inhibitor and the charged metal; while the value of ΔG_{ads} is close to or higher than $40 \text{ kJ}\cdot\text{mol}^{-1}$, the chemical adsorption occurred between the inhibitor and the Fe metal surface. When the value of ΔG_{ads} was between $20\text{--}40 \text{ kJ}\cdot\text{mol}^{-1}$, both physical and chemical adsorption occurred [33]. From the data calculated

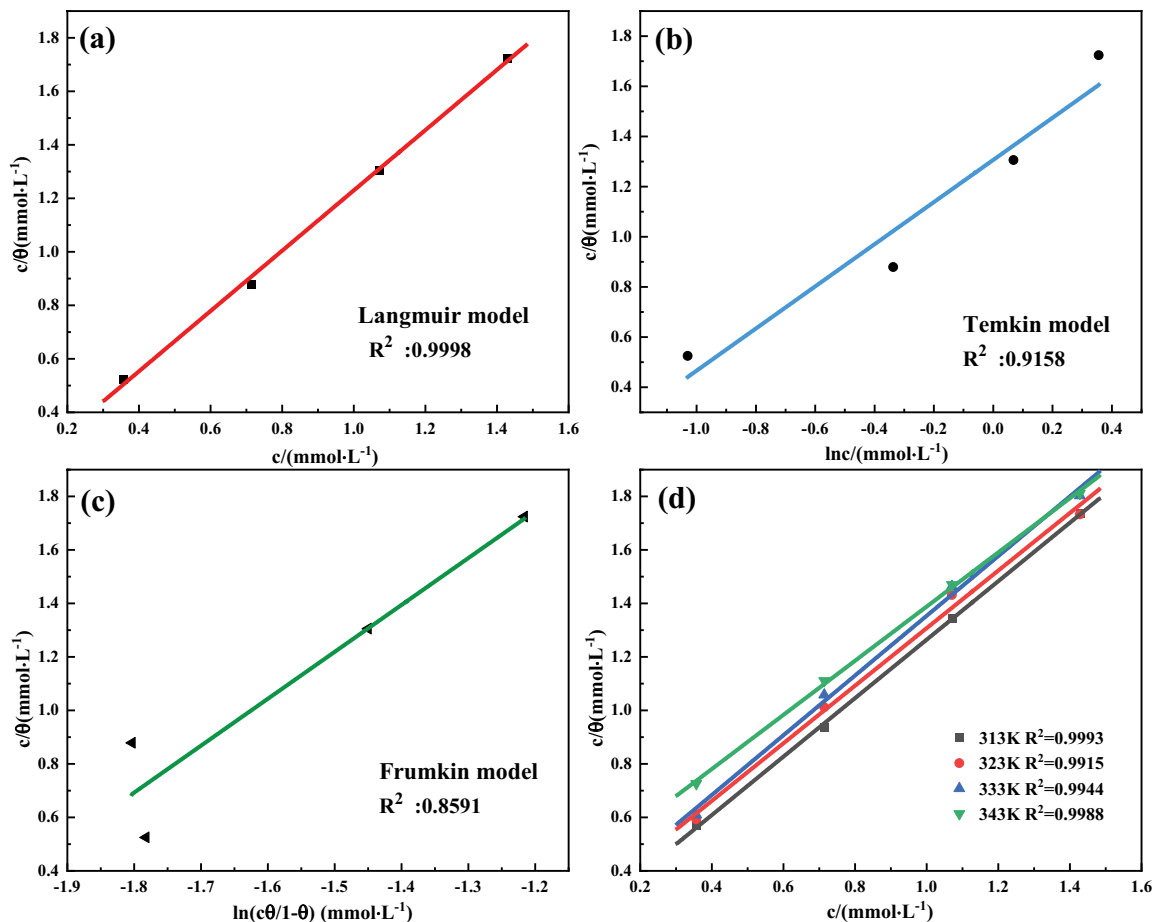


Fig. 9. Adsorption fitting results of different models.

in Table 5, it can be seen that the values of free energy of adsorption (ΔG_{ads}) at different temperatures are around $-33 \text{ kJ}\cdot\text{mol}^{-1}$. This indicated that in the simulated corrosive medium HTCI corrosion inhibitor on the surface of the steel sheet, there was physical adsorption as well as chemical adsorption.

$$\Delta G_{\text{ads}} = -RT \ln(55.5K) \quad (8)$$

The absolute value of ΔG_{ads} decreased to a limited extent with increasing temperature. Thermodynamically, ΔG_{ads} is related to ΔH_{ads} (standard enthalpy) and ΔS_{ads} (standard entropy) of the adsorption process and the value of ΔH_{ads} was determined by the van't Hoff Eq. (9) with $\ln(55.5 \text{ K})$ and $1/T$. As shown in Fig. 10, the $\ln(55.5 \text{ K})$ and $1/T$ fits were

Table 5
Kinetic parameters for the adsorption of HTCI on the mild steel

| Temperature (K) | R^2 | Slope | $K (\times 10^3)$ | $\Delta G_{\text{ads}} (\text{kJ}\cdot\text{mol}^{-1})$ |
|-----------------|--------|--------|-------------------|---|
| 303 | 0.9998 | 1.1272 | 9.7634 | -33.26 |
| 313 | 0.9993 | 1.0929 | 5.8295 | -33.02 |
| 323 | 0.9915 | 1.0761 | 4.3209 | -33.27 |
| 333 | 0.9944 | 1.1163 | 3.7400 | -33.90 |
| 343 | 0.9988 | 1.0123 | 2.6607 | -33.94 |

Table 6
Thermodynamic parameters for the adsorption of HTCI on the mild steel

| $c (\text{mg}\cdot\text{L}^{-1})$ | A | $E_a (\text{kJ}\cdot\text{mol}^{-1})$ | $\Delta H_a (\text{kJ}\cdot\text{mol}^{-1})$ | $\Delta S_a (\text{J}\cdot\text{mol}^{-1}\cdot\text{K}^{-1})$ |
|-----------------------------------|------|---------------------------------------|--|---|
| 0 | 0.22 | 10.86 | 6.85 | -270.80 |
| 100 | 0.79 | 16.91 | 10.71 | -267.25 |
| 200 | 0.95 | 18.63 | 16.36 | -252.98 |
| 300 | 0.85 | 18.56 | 15.22 | -257.35 |
| 400 | 0.06 | 11.98 | 8.71 | -257.38 |

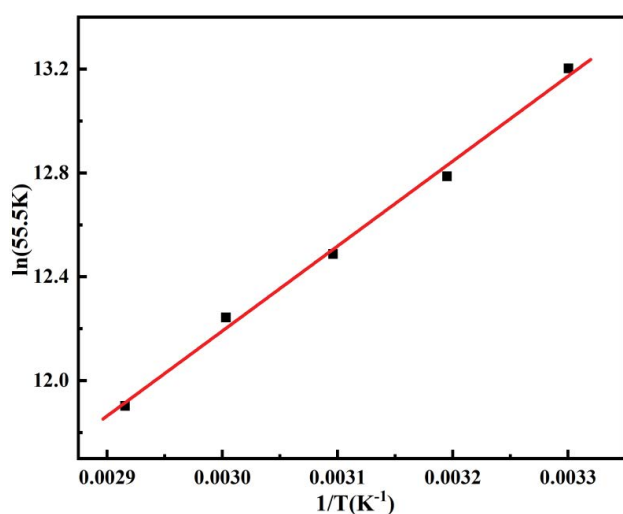


Fig. 10. Van't Hoff plot for the mild steel.

linear ($R_2 = 0.9935$), where the slope was $-\Delta H_a/R$, and the standard enthalpy of adsorption $\Delta H_{\text{ads}} = -27.20 \text{ kJ}\cdot\text{mol}^{-1}$ was calculated. The value of ΔS_{ads} was calculated from Eq. (10). The standard entropy of adsorption $\Delta S_{\text{ads}} = -20.66 \text{ J}\cdot\text{mol}^{-1}\cdot\text{K}^{-1}$. In exothermic processes, a distinction is made between chemisorption and physisorption by considering the absolute value of ΔH_{ads} and ΔS_{ads} . For chemisorption processes, ΔH_{ads} is close to $100 \text{ kJ}\cdot\text{mol}^{-1}$, whereas for physical adsorption processes it is less than $40 \text{ kJ}\cdot\text{mol}^{-1}$ [34]. In this experiment, the ΔH_{ads} values were lower than normal enthalpy of physical adsorption, indicating that the adsorption of HTCI on carbon steel surfaces was dominated by physical adsorption.

$$\ln(55.5K) = \frac{-\Delta H_{\text{ads}}}{RT} + \frac{\Delta S_{\text{ads}}}{R} \quad (9)$$

$$\Delta G_{\text{ads}} = \Delta H_{\text{ads}} - T\Delta S_{\text{ads}} \quad (10)$$

3.7. Thermodynamic adsorption parameters

The surface of the metal intricately changed at different temperature, and thermodynamic parameter calculations were used to infer the mechanism of action of the corrosion inhibitor. Further parametric simulations were made using the Arrhenius Eq. (11) [35].

Arrhenius equation:

$$C_v = A \exp\left(-\frac{E_a}{RT}\right) \quad (11)$$

Derivation of the transition state equation:

$$\ln C_v = \ln A - \frac{E_a}{RT} \quad (12)$$

$$C_v = \frac{RT}{Nh} \exp\left(\frac{\Delta S_a}{R}\right) \exp\left(-\frac{\Delta H_a}{RT}\right) \quad (13)$$

where C_v denotes the corrosion rate constant; A refers to the Arrhenius finger prefactor; E_a is the apparent activation energy; $R = 8.314 \text{ J}\cdot\text{K}^{-1}\cdot\text{mol}^{-1}$; T is the absolute temperature; h is Planck's constant, $h = 6.626176 \times 10^{-34} \text{ Js}$; N is Avogadro's constant, $N = 6.02252 \times 10^{23} \text{ mol}^{-1}$; ΔS_a is the entropy of activation and ΔH_a is the enthalpy of activation [36].

Fig. 11 shows the Arrhenius curve for the corrosion rate of carbon steel and Fig. 12 shows transition-state plots for mild steel with different concentrations. The values of E_a , ΔH_a and ΔS_a were calculated from Table 6. As shown in Table 6, the thermodynamic parameters of HTCI adsorption on mild steel and the activation energy E_a had a trend of increasing and then decreasing. A decrease of E_a indicated the presence of chemical adsorption of HTCI at the interface between the steel sheet and the solution and an increase of E_a indicated the presence of physical adsorption of HTCI. Therefore, it can be demonstrated that both physical and chemical adsorption of HTCI existed at the steel-solution interface. In the presence of HTCI, higher values of ΔS_a indicated an increase in the entropy of the solvent. This may be due to the desorption of a large number

of molecules already adsorbed on the metal surface and the less disordered adsorption of the larger tartaric acid and hydrazine hydrate molecules on the carbon steel surface.

3.8. Microscopic morphology of corrosion surface

The surface of the steel sheet of corrosion in saturated $\text{Ca}(\text{OH})_2$ solution containing 3.0 wt.% NaCl after 14 d was

scanned by fully automatic 3D imaging microscope, and the same point of the Q235 specimen was magnified 75, 100, 200 and 300 times in the area of the etch pits, respectively. The scanned 2D, height and 3D images are displayed in Fig. 13. The depths of pitting pits measured at different magnifications were $457.524 \mu\text{m}$ ($\times 75$), $493.889 \mu\text{m}$ ($\times 100$), $505.559 \mu\text{m}$ ($\times 200$), and $548.729 \mu\text{m}$ ($\times 300$), respectively.

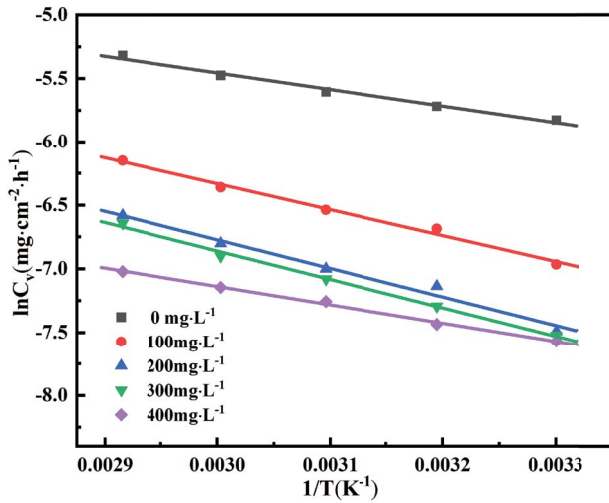


Fig. 11. Arrhenius plots of HTCI with different concentrations.

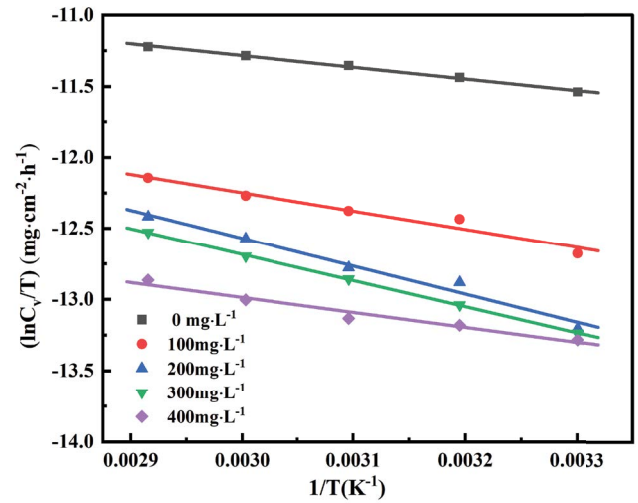


Fig. 12. Transition-state plots for mild steel with different concentrations.

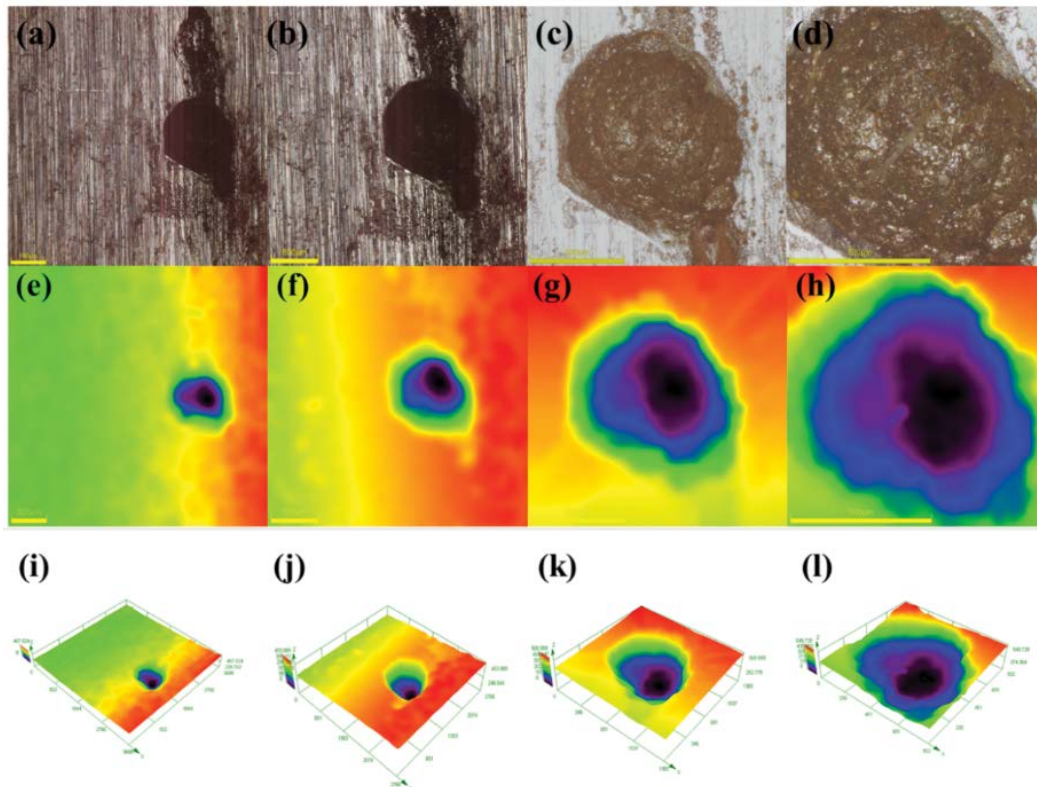


Fig. 13. 2D (a–d), height (e–h), 3D (i–l) images of Q235 specimens at different magnifications (magnification from left to right: 75, 100, 200 and 300 times).

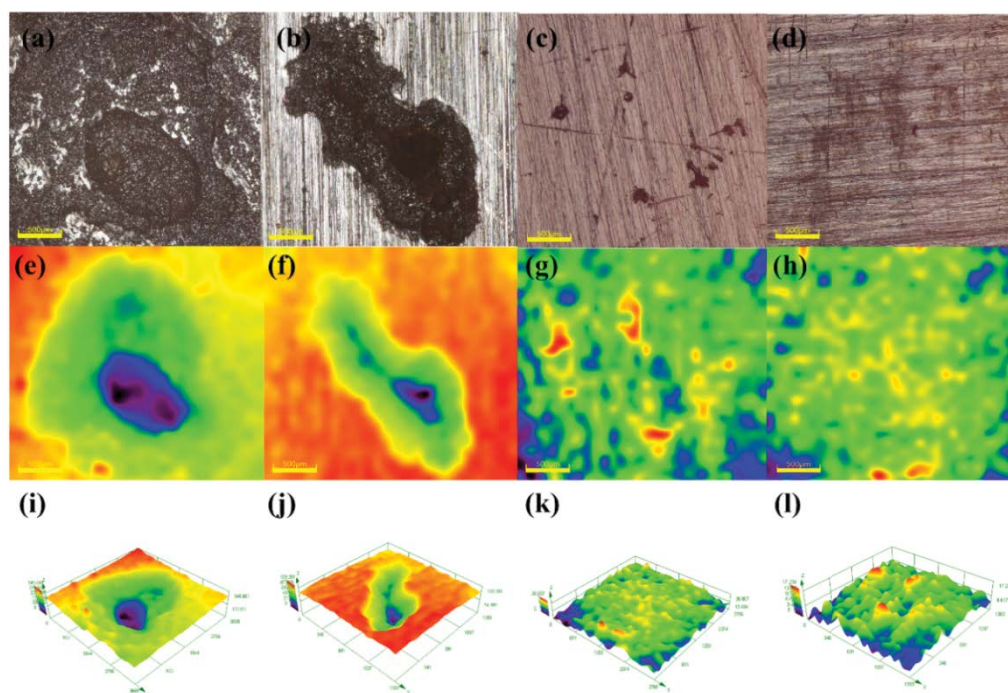


Fig. 14. 2D (a–d), height (e–h), 3D (i–l) images of specimens at 200 magnification after addition of different concentrations of HTCI (from top to bottom, HTCI added at 100, 200, 300 and 400 $\text{mg}\cdot\text{L}^{-1}$).

The images of Q235 carbon steel specimens were magnified to 200 times by observing the height map to measure the surface as well as the depth of the pitting pits, and no obvious faults appeared around the images. Combining the integrity of the image and the degree of overlap, the pitting depth at 200 times magnification was chosen as the maximum pitting pit depth with a value of 505.229 μm .

For Q235 carbon steel specimens, HTCI inhibitor at concentrations of 100, 200, 300, and 400 $\text{mg}\cdot\text{L}^{-1}$ was added to a saturated $\text{Ca}(\text{OH})_2$ solution containing 3.0 wt.% NaCl at 30°C and removed after 14 d of corrosion. The specimens were scanned in 2D and 3D images as well as height maps at 200 magnification, as shown in Fig. 14. From the 2D images, with the increase of HTCI concentration, the corrosion condition of carbon steel surface, the range of pitting pits, and the roughness significantly decreased. The steel surface became smoother, the pitting pits disappeared, and only some corrosion scratches existed on the steel surface at the HTCI concentration of 400 $\text{mg}\cdot\text{L}^{-1}$, from the height map. The maximum pitting depths were 345.660, 109.381, 26.807 and 17.234 μm , respectively, as seen from the 3D images at different concentrations, and the depth of pitting pits decreased gradually with the increase of HTCI concentration, which proved that HTCI effectively suppressed the occurrence of pitting corrosion.

4. Conclusion

In this paper, a composite corrosion inhibitor (HTCI) was successfully prepared by the complex reaction of tartaric acid and hydrazine hydrate. The result of weight loss measurements showed a maximum inhibition of 84.37% when the reaction time was 7 d, the temperature was at

303 K, the concentration was 500 $\text{mg}\cdot\text{L}^{-1}$ and the corrosion rate was 0.00524 $\text{mm}\cdot\text{a}^{-1}$; the maximum inhibition rate was 85.41% when the corrosion time reached 30 d. Potentiodynamic polarization studies showed that HTCI was an effective inhibitor of mild steel corrosion in saturated $\text{Ca}(\text{OH})_2$ solution with 3.0 wt.% NaCl. Impedance studies showed that the capacitive arc radius gradually increases, the double layer thickness increased, the dispersion index decreased and the corrosion resistance was enhanced with the gradual increase of HTCI concentration. Furthermore, the adsorption of HTCI on the surface of Q235 steel plate conformed to the Langmuir adsorption through kinetic and thermodynamic simulations. By scanning the surface of the corroded steel plate, the depth of pitting pits gradually decreased with the increase of HTCI concentration. The maximum depth of pitting pits on the surface of Q235 carbon steel specimens after 14 d of corrosion in saturated $\text{Ca}(\text{OH})_2$ solution containing 3.0 wt.% NaCl was 505.229 μm , and the maximum depth of pitting pits after the addition of 400 $\text{mg}\cdot\text{L}^{-1}$ of HTCI resulted in a maximum pitting pit depth of 17.234 μm .

Acknowledgments

The work was supported financially by the Key Projects of China National Key R&D Plan (2021YFE0107000), National Natural Science Foundation of China (52074339), Key Scientific Research Program of Shaanxi Provincial Department of Education (22JY052), Postgraduate Innovation Fund Project of Xi'an Shiyou University (YCS22213095) and Youth Innovation Team of Shaanxi University. The authors also thank the Center of Advanced Analysis and Testing at Xi'an Shiyou University for their work.

References

- [1] M.F. Montemor, A.M.P. Simões, M.G.S. Ferreira, Chloride-induced corrosion on reinforcing steel: from the fundamentals to the monitoring techniques, *Cem. Concr. Compos.*, 25 (2003) 491–502.
- [2] L. Mammoliti, C.M. Hansson, B.B. Hope, Corrosion inhibitors in concrete Part II: effect on chloride threshold values for corrosion of steel in synthetic pore solutions, *Cem. Concr. Compos.*, 29 (1999) 1583–1589.
- [3] S.A. Mangi, A. Makhija, M.S. Raza, S.H. Khahro, A.A. Jhatal, A comprehensive review on effects of seawater on engineering properties of concrete, *Silicon*, 13 (2021) 4519–4526.
- [4] W.K. Green, Steel reinforcement corrosion in concrete – an overview of some fundamentals, *Corros. Eng. Sci. Technol.: Int. J. Corros. Processes Corros. Control*, 55 (2020) 289–302.
- [5] B. Fabio, B. Andrea, O. Marco, Recent advances in the use of inhibitors to prevent chloride-induced corrosion in reinforced concrete, *Cem. Concr. Res.*, 154 (2022) 106719, doi: 10.1016/j.cemconres.2022.106719.
- [6] P.B. Raja, Pitchumani, Corrosion mitigation in reinforced concrete structures using protective coatings—a review, *J. Coat. Technol. Res.*, 15 (2001) 1013–1033.
- [7] H.-h. Zhang, X. Pang, K. Gao, Localized CO₂ corrosion of carbon steel with different microstructures in brine solutions with an imidazole-based inhibitor, *Appl. Surf. Sci.*, 442 (2018) 446–460.
- [8] R.E. Melchers, Long-term durability of marine reinforced concrete structures, *J. Mar. Sci. Eng.*, 8 (2020) 290, doi: 10.3390/jmse8040290.
- [9] H. Jafari, K. Akbarzade, I. Danaee, Corrosion inhibition of carbon steel immersed in a 1 M HCl solution using benzothiazole derivatives, *Arabian J. Chem.*, 12 (2019) 1387–1394.
- [10] A.U. Malik, I. Andijani, F. Al-Moaili, G. Ozair, Studies on the performance of migratory corrosion inhibitors in protection of rebar concrete in Gulf seawater environment, *Cem. Concr. Compos.*, 26 (2004) 235–242.
- [11] A. Saxena, D. Prasad, R. Haldhar, Use of *Syzygium aromaticum* extract as green corrosion inhibitor for mild steel in 0.5 M H₂SO₄, *Surf. Rev. Lett.*, 53 (2019) 8523–8535.
- [12] P.B. Raja, S. Ghoreishiamiri, M. Ismail, Natural corrosion inhibitors for steel reinforcement in concrete – a review, *Surf. Rev. Lett.*, 22 (2015) 8, doi: 10.1142/S0218625X15500407.
- [13] S.G. Dong, B. Zhao, C. Lin, R.G. Du, R.G. Hu, G.X. Zhang, Corrosion behavior of epoxy/zinc duplex coated rebar embedded in concrete in ocean environment, *Constr. Build. Mater.*, 28 (2012) 72–78.
- [14] S.J. Li, C.W. Guo, X. Wang, C. Guan, G. Chen, Corrosion inhibition coating based on the self-assembled polydopamine films and its anti-corrosion properties, *Polymers*, 14 (2022) 794, doi: 10.3390/polym14040794.
- [15] GB/T 19291-2003 Corrosion of Metals and Alloys – General Principles for Corrosion Testing, China National Petroleum Corporation, Beijing, 2003.
- [16] D. Yang, Y. Ye, Y. Su, S. Liu, D. Gong, H. Zhao, Functionalization of citric acid-based carbon dots by imidazole toward novel green corrosion inhibitor for carbon steel, *J. Cleaner Prod.*, 229 (2019) 180–192.
- [17] X. Gu, H.N. Zhang, W.C. Du, Z.F. Zhang, S.D. Zhu, G. Chen, Modification and application of walnut peel extract as acidic corrosion inhibitor, *J. Biobased Mater. Bioenergy*, 15 (2021) 820–825.
- [18] S. Hari Kumar, S. Karthikeyan, Amoxicillin as an efficient green corrosion inhibitor for mild steel in 1M sulphuric acid, *J. Mater. Environ. Sci.*, 4 (2013) 675–684.
- [19] F. Bentiss, M. Lagrenee, M. Traisnel, J.C. Hornez, The corrosion inhibition of mild steel in acidic media by a new triazole derivative, *Corros. Sci.*, 41 (1999) 789–803.
- [20] H. Ashassi-Sorkhabi, N. Ghalebsaz-Jeddi, F. Hashemzadeh, H. Jahani, Corrosion inhibition of carbon steel in hydrochloric acid by some polyethylene glycols, *Electrochim. Acta*, 51 (2005) 3848–3854.
- [21] I.B. Obot, N.O. Obi-Egbedi, Adsorption properties and inhibition of mild steel corrosion in sulphuric acid solution by ketoconazole: experimental and theoretical investigation, *Corros. Sci.*, 52 (2010) 198–204.
- [22] A.K. Singh, S. Khan, S. Aditya, S.M. Quraishi, M.A. Quraishi, E.E. Ebenso, Inhibitive effect of chloroquine towards corrosion of mild steel in hydrochloric acid solution, *Res. Chem. Intermed.*, 39 (2013) 1191–1208.
- [23] F. Bentiss, M. Traisnel, M. Lagrenee, Inhibitor effects of triazole derivatives on corrosion of mild steel in acidic media, *Br. Corros. J.*, 35 (2000) 315–320.
- [24] N.O. Eddy, P.O. Ameh, C.E. Gimba, E.E. Ebenso, Rheological modeling and characterization of *Ficus platyphylla* gum exudates, *J. Chem.*, 2013 (2013) 254347, doi: 10.1155/2013/254347.
- [25] C.O. Akalezi, A.C. Maduabuchi, C.K. Enenebeaku, E.E. Oguzie, Experimental and DFT evaluation of adsorption and inhibitive properties of *Moringa oleifera* extract on mild steel corrosion in acidic media, *Arabian J. Chem.*, 13 (2020) 9270–9282.
- [26] Y. Bai, J. Zhang, S. Dong, J. Li, R. Zhang, C. Pu, G. Chen, Effect of anion on the corrosion inhibition of cationic surfactants and a mechanism study, *Desal. Water Treat.*, 188 (2020) 130–139.
- [27] X. Gu, K. Dong, J. Tian, H. Li, J. Zhang, C.T. Qu, G. Chen, Investigation of modified *Ginkgo biloba* leaves extract as eco-friendly inhibitor for the corrosion of N80 steel in 5% HCl, *Desal. Water Treat.*, 107 (2018) 118–126.
- [28] S.-D. Zhu, Y.-P. Li, H.-W. Wang, J.-L. Li, A.-Q. Fu, G. Chen, D. Ma, X.-P. Li, F. Cheng, Corrosion resistance mechanism of mica-graphene/epoxy composite coating in CO₂-Cl⁻ system, *Materials (Basel)*, 15 (2022) 1194, doi: 10.3390/ma15031194.
- [29] L.A. Al Juhaïman, A.A. Mustafa, W.K. Mekhamer, Polyvinyl pyrrolidone as a green corrosion inhibitor for carbon steel in alkaline solutions containing NaCl, *Anti-Corros. Methods Mater.*, 60 (2013) 28–36.
- [30] Q. Liu, M. Gao, Y. Zhao, J. Li, C. Qu, J. Zhang, G. Chen, Synthesis and interfacial activity of a new quaternary ammonium surfactant as an oil/gas field chemical, *Tenside, Surfactants, Deterg.*, 57 (2020) 90–96.
- [31] A.M. Mustafa, F.F. Sayyid, N. Betti, L.M. Shaker, M.M. Hanoon, A.A. Alamiery, A.A.H. Kadhum, M.S. Takriff, Inhibition of mild steel corrosion in hydrochloric acid environment by 1-amino-2-mercapto-5-(4-(pyrrol-1-yl)phenyl)-1,3,4-triazole, *S. Afr. J. Chem. Eng.*, 39 (2022) 42–51.
- [32] M.S. Zandi, M. Hasanazadeh, The self-healing evaluation of microcapsule-based epoxy coatings applied on AA6061 Al alloy in 3.5% NaCl solution, *Anti-Corros. Methods Mater.*, 64 (2017) 225–232.
- [33] A. Ghanbari, M.M. Attar, M. Mahdavian, Corrosion inhibition performance of three imidazole derivatives on mild steel in 1 M phosphoric acid, *Mater. Chem. Phys.*, 124 (2010) 1205–1209.
- [34] P. Wang, X. Gu, Q. Wang, J.L. Dong, S.B. Dong, J. Zhang, S.D. Zhu, G. Chen, Corrosion inhibition of triazines in sulfur-containing oilfield wastewater, *Desal. Water Treat.*, 235 (2021) 107–116.
- [35] A. Kokalj, S. Peljhan, M. Finšgar, I. Milošev, What determines the inhibition effectiveness of ATA, BTAH, and BTAOH corrosion inhibitors on copper, *J. Am. Chem. Soc.*, 132 (2010) 16657–16668.
- [36] G. Chen, Y. Bai, Q. Liu, J. Zhang, X. Gu, H. Li, C. Qu, Y. Zhang, Synthesis and interface activity of a series of dicarboxylic cationic surfactants and a structure–efficiency relationship study, *J. Surfactants Deterg.*, 22 (2019) 691–698.